SA738Gr. B 钢焊接热影响区组织及性能的热模拟试验

丁连征[1]， 王 锴[2]， 孟庆森[1]
(1. 太原理工大学 材料学院，太原 030024；2. 机械科学研究院 哈尔滨焊接研究所，哈尔滨 150001)

摘 要：采用热膨胀的方法测定了钢制安全壳用钢 SA738Gr. B 在不同冷却速度下的组织转变，采用 GLEEBLE-2000 试验机模拟分析了焊接参数对热影响区组织及冲击韧性的影响，进行了实际焊接，验证了与实际组织的相一致性. 结果表明，随冷却速度的降低，SA738Gr. B 钢板先后发生贝氏体转变、先共析铁素体析出及先共析铁素体 + 珠光体组织的转变. 多层多道焊时，实际热影响区组织以混合组织为主，其基体组织基本符合同冷却速度条件下的热模拟组织，具有较高的抗裂性能. 研究结果对生产实践具有较好的参考和指导作用.

关键词：SA738Gr. B 钢；热模拟；热影响区；力学性能
中图分类号：TG 401 **文献标识码**：A **文章编号**：0253 - 360X(2014)08 - 0091 - 04

0 序 言

SA738Gr. B 钢板是首次用于国内第三代核电 AP1000 钢制安全壳制造的低合金调质钢. 由于焊后不再进行热处理，热影响区的性能倍受关注[1,2]. 因为焊缝性能可通过焊接材料的选择来改善，而对于焊后不再进行热处理的焊接件其热影响区的性能只能通过工艺参数来调整改善[3,4,5]. 随着焊接结构向高参数、大型化的发展，热影响区性能对焊接结构的质量及其安全运行的影响越来越大[5,6]. 由于实际焊接热影响区狭窄，精确地研究实际焊件热影响区性能几乎是不可能的. 文中采用热膨胀法研究了 SA738Gr. B 钢板在不同冷却速度时的组织转变，采用 GLEEBLE-2000 试验机模拟了焊接时 SA738Gr. B 钢接头的热影响区组织及冲击韧性的变化. 分析了不同焊接冷却速度对该钢热影响区微观组织及冲击韧性的影响，为该钢的生产及推广应用提供了试验依据.

1 试验方法

试验采用国内某大型钢铁集团生产的 SA738Gr. B 钢板，厚度为 42.1 mm，其含碳量控制很低，不大于 0.08%，碳当量约在 0.45%，S 元素含量 0.006 8%，P 元素含量 0.001 4%，供货状态为调质，回火 630 ℃ ×0.5 h，供货状态下的组织为贝氏体组织[7]. 供货状态下的抗拉强度、屈服强度分别为 639 和 562 MPa，-29 ℃的冲击吸收功分别为 266，194，277 J.

根据冶金行业标准 YB/T5127—1993《钢的临界点测定方法》测定钢的临界转变温度点. 测试结果表明，SA738Gr. B 钢奥氏体转变开始温度 A_{C_1} 约为 707 ℃，奥氏体转变的终了温度 A_{C_3} 约为 858 ℃.

按照冶金行业标准 YB/T5128—1993《钢的连续冷却转变曲线的测定方法》，采用 Formaster-D 全自动快速膨胀仪对 SA738Gr. B 钢在不同热循环条件下的热影响区组织转变进行研究与测定. 根据相关研究结果[1] 及实际焊接加热与冷却速度，确定如下的热模拟参数：以 200 ℃/s 的加热速度从室温升至峰值温度 1 320 ℃，停留 2 s，峰值温度至 900 ℃(858 ℃) 的冷却速度为 40 ℃/s. 然后各试样从 900 ℃以不同速度冷却到室温，记录 $t_{8/5}$ 的值，全部试样按上述参数模拟焊接热循环，并将不同冷却速度下的热模拟试样制备成金相试样，用 4% 硝酸酒精侵蚀，分析不同冷却速度下的微观组织，如图 1 所示. 组织、硬度与冷却速度关系如表 1 所示.

采用 GLEELE-2000 试验机模拟了热影响区不同冷却速度下不同区域的韧性值. 为测试热模拟与焊件热影响区异同，实测了焊件热影响区. 试板 SA738Gr. B 尺寸为 500 mm × 125 mm × 42.1 mm，60°坡口，KEPPI PRO450 焊机，焊丝 ER90S-G/ϕ1.2. 采用不同的热输入，不预热的条件下，采用微机控制的接触式热电偶测量 $t_{8/5}$ 时间. 焊接工艺参数：打底焊焊接电流 140 ~ 150 A，电弧电压 19 ~ 22 V，焊接速度 20 ~ 25 cm/min. 填充焊焊接电流 200 ~ 220 A，电弧电压 25 ~ 28 V，焊接速度 30 ~ 40 cm/min，控制

收稿日期：2014 - 05 - 20

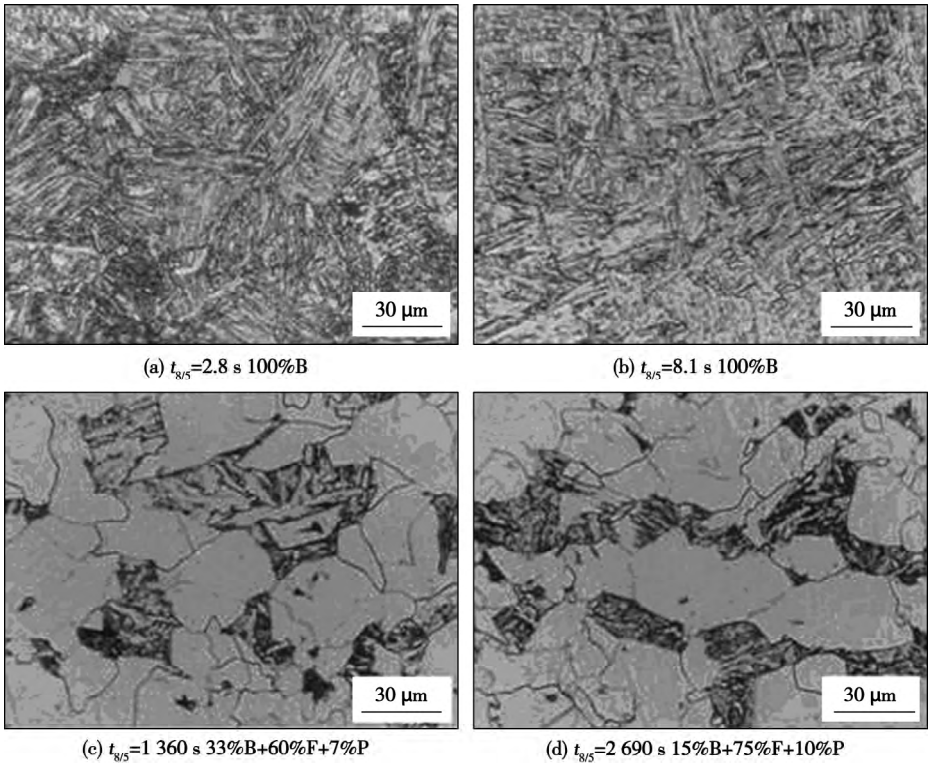

(a) $t_{8/5}$=2.8 s 100%B (b) $t_{8/5}$=8.1 s 100%B

(c) $t_{8/5}$=1 360 s 33%B+60%F+7%P (d) $t_{8/5}$=2 690 s 15%B+75%F+10%P

图 1 不同 $t_{8/5}$ 时的组织变化

Fig. 1 Microstructure at different $t_{8/5}$

表 1 $t_{8/5}$ 与 SA738Gr. B 钢的组织及硬度关系

Table 1 The relationship among $t_{8/5}$ and microstructure and the hardness

编号	冷却时间 $t_{8/5}$/s	维氏硬度 H_{HV5}/MPa	质量分数 w(%)	临界冷却时间 t/s
1	2.8	270	100% B	
2	5.2	268	100% B	
3	8.1	250	100% B	
4	24	231	100% B	
5	75	222	100% B	t_{fs} = 195
6	116	207	100% B	t_{ps} = 330
7	224	200	90% B + 10% F	
8	510	194	58% B + 30% F + 12% P	
9	1 360	186	33% B + 60% F + 7% P	
10	2 690	177	15% B + 75% F + 10% P	

注: t_{fs} 为铁素体开始转变的临界冷却时间; t_{ps} 为珠光体开始转变的临界冷却时间

层间温度不低于 120 ℃. 经实际测量,在控制层间温度的情况下冷却时间在 6 ~ 25 s 之间. 对焊接热影响区和模拟热影响区进行了比较.

2 试验结果及分析

2.1 连续冷却速度对组织的影响

不同的冷却速度下,奥氏体主要发生两种转变,奥氏体转变为贝氏体(A→B)、先共析铁素体珠光体混合物的转变(A→F + P).

由表 1 可见,即使冷却速度较快时($t_{8/5}$ 为 2.8 s),组织中无马氏体转变,转变主要发生在中高温之间. 这主要是由于 SA738Gr. B 钢中碳含量、合金含量控制得低,使得等温转变曲线向左移动,更易发生高中温转变,所以不易出现马氏体. 欲得到马氏体组织,需要在更低冷却速度下进行,SA738Gr. B 钢的淬硬倾向较小. 贝氏体组织转变范围很宽,从 2.8 s 到 195 s 的范围内,全部为贝氏体组织转变区域. 由于冷却速度的不同,其组织形态大不相同,当 $t_{8/5}$ 在 2.8 s 时,贝氏体板极细,冷却速度越快,过冷度越大,形核功越大,晶粒越细. 随着冷却速度的变慢即 $t_{8/5}$ 的增加,板条变宽,比较图 1a,b 可以清晰看到图 1b 板条变粗,有的地方甚至相互交联在一起.

当 $t_{8/5}$ > 195 s 时,有先共析铁素体析出,从图 1c 可见,先共析铁素体从原晶界析出,呈点状分布,随着冷却速度的变慢,铁素体逐渐成块状析出,并且有珠光体生成,二者混合在一起. 冷却速度越慢,含量越多如图 1d. 相应地随着冷却速度的降低,硬度值呈现下降的趋势,在冷却速度较大时,以贝氏体转变为主,其具有较高的硬度,而 $t_{8/5}$ 较大时,冷却速度低,先共析铁素体含量多,造成硬度降低.

2.2 连续冷却速度对力学性能的影响

连续冷却速度对力学性能的影响见表 2. 热影

响区分成三个不同的峰值温度区（1 320，920，800 ℃），可见峰值温度和 $t_{8/5}$ 时间对热影响区韧性的冲击值有显著影响. 过热区高温停留时间长，峰值温度高，晶粒变粗造成冲击韧性下降；过热区和不完全相变区虽能满足冲击韧性不低于 47 J 的要求，但波动较大；不完全相变区发生了部分奥氏体化，保留了部分原始组织，晶粒粗细不均，造成了韧性较低；正火区由于受热温度稍高于 A_{C_3}，奥氏体晶粒基本维持原晶粒大小，在空气中冷却生成更加细小的二次组织，所以该区冲击韧性良好.

表 2　不同焊接热循环条件下 SA738Gr. B 钢热影响区冲击吸收功

Table 2　Relationship among $t_{8/5}$ microstructure and hardness

序号	峰值温度 T_p /℃	峰值温度停留时间 t /s	V 形缺口在热影响区位置	冷却时间 $t_{8/5}$ /s	冲击吸收功 $A_{KV(-29\ ℃)}$ /J
11	1 320	0.5	过热区	5	51
12	1 320	0.5	过热区	10	104
13	1 320	0.5	过热区	15	94
14	1 320	0.5	过热区	20	97
15	1 320	0.5	过热区	25	85
16	1 320	0.5	过热区	30	47
21	920	0.5	正火区	5	263
22	920	0.5	正火区	10	278
23	920	0.5	正火区	15	239
24	920	0.5	正火区	20	261
25	920	0.5	正火区	25	232
26	920	0.5	正火区	30	194
31	800	0.5	不完全相变区	5	64
32	800	0.5	不完全相变区	10	107
33	800	0.5	不完全相变区	15	177
34	800	0.5	不完全相变区	20	76
35	800	0.5	不完全相变区	25	54
36	800	0.5	不完全相变区	30	49

2.3　实际焊接件 HAZ 组织和性能的比较

为分析实际焊接时 HAZ 的组织转变与热模拟试验的一致性，实测了气体保护焊在焊接条件下热影响区冲击韧性. 焊接时由于不预热，打底焊道全是冷金属，冷却速度快，$t_{8/5}$ 在 6 ~ 10 s 之间，填充焊道由于控制层间温度不低于 120 ℃，且由于热输入的不同，热影响区的实际冷却时间 $t_{8/5}$ 在 10 ~ 25 s 之间，各区对应的组织和冲击韧性分别见图 2 和表 3. 比较表 2 可见实际焊件的冲击韧性远高于热模拟试验各区的韧性值，由组织分析可知，实际焊接条件下的热影响区组织变化与热模拟获得的组织有部分差异. 气体保护焊的热影响区组织主要以贝氏体为主，基本同模拟结果相似. 热模拟以单次热循环为研究对象，而实际焊接时一般为多层多道焊，后一焊道对前一焊道有重热作用，可以通过再结晶使金相组织细化. 相比热模拟试验，由于实际焊接时热影响区涵盖了从高到低全部焊接热循环范围. 金相组织呈逐渐变化，呈现脆性较大的区域往往很窄，而冲击试样缺口下往往包含了不同峰值温度的组织，所以韧性往往要比脆性区模拟热循环试样要高. 其韧性值更接近于各区的平均值，这在工程上是可以接受的[8].

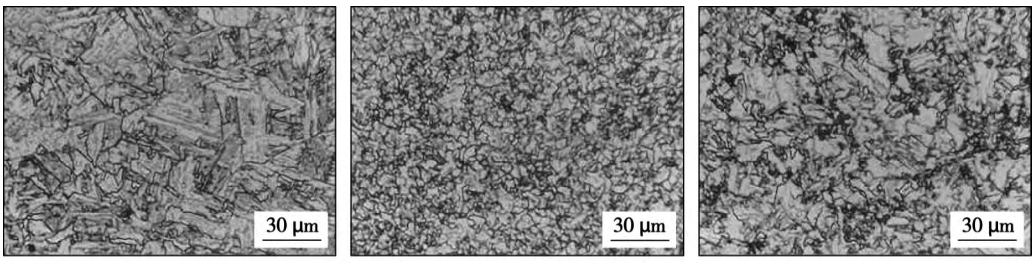

(a) 过热区　(b) 正火区　(c) 不完全相变区

图 2　气体保护焊热影响区形貌

Fig. 2　HAZ microstructure for GMAW process

表 3 不同热输入时热影响区冲击吸收功

Table 3 Impact toughness for HAZ at different heat input

试件编号	热输入 E/(kJ·mm^{-1})	缺口位置	试验温度 T/℃	冲击吸收功 A_{KV}/J
11	1.2	熔合线	-29	198
13	1.2	熔合线外 3 mm	-29	235
14	1.2	熔合线外 5 mm	-29	251
21	1.6	熔合线	-29	261
23	1.6	熔合线外 3 mm	-29	227
24	1.6	熔合线外 5 mm	-29	293
31	2.0	熔合线	-29	105
33	2.0	熔合线外 3 mm	-29	201
34	2.0	熔合线外 5 mm	-29	243

3 结 论

(1) SA738Gr. B 钢的测定结果表明,在较宽的冷却速度范围内,热影响区依次发生贝氏体、先共析铁素体 + 贝氏体组织、先共析铁素体 + 珠光体 + 贝氏体组织的转变. 通过这些数据可以绘制焊接连续冷却曲线(SHCCT),SHCCT 曲线是指导生产的技术依据.

(2) 峰值温度和 $t_{8/5}$ 时间对热影响区各区的冲击韧性有显著影响. 过热区高温停留时间长,晶粒变粗造成冲击韧性下降; 不完全相变区保留了部分原始组织,晶粒粗细不均,韧性较低; 正火区晶粒基本维持原晶粒大小,冷却过程生成更加细小的二次组织,冲击韧性良好.

(3) 实际焊接条件下的多层多道焊后焊道对前焊道有回火作用,热影响区晶粒比单道焊时晶粒细小,性能优于单道焊.

参考文献:

[1] 张文钺. 焊接冶金学[M]. 北京: 机械工业出版社, 1999.

[2] 李为卫, 刘亚旭, 高惠临, 等. X80 管线钢焊接热影响区的韧性分析[J]. 焊接学报, 2009, 30(1): 109 - 112.
Li Weiwei, Liu Yaxu, Gao Huilin, *et al*. Analysis of toughness in HAZ for X80 pipeline steel welding[J]. Transactions of the China Welding Institution, 2009, 30(1): 109 - 112.

[3] 屈朝霞, 田志凌, 何长虹, 等. 超细晶粒钢及其焊接性[J]. 钢铁, 2000, 35(2): 70 - 73.
Qu Zhaoxia, Tian Zhiling, He Changhong, *et al*. Ultra-fine grained steel and its weldability[J]. Iron and Steel, 2000, 35(2): 70 - 73.

[4] 胡淑娥, 孙卫华, 侯东华. 700 MPa 级高强钢焊接接头与组织[J]. 材料热处理学报, 2013, 34: 71 - 76.
Hu Sue, Sun Weihua, Hou Donghua, *et al*. Properties and microstructure of welded joint of 700 MPa grade high strength steel[J]. Transactions of Materials and Heat Treatment, 2013, 34: 71 - 76.

[5] 荆洪阳, 马 崇, 樊立国, 等. TMCP 钢焊接热影响区局部脆化区断裂韧度测试[J]. 焊接学报, 2004, 30(3): 19 - 23.
Jing Hangyang, Ma Chong, Fan Liguo, *et al*. Investigation on measurement of fracture toughness for local brittle zone in weld heat-affected zone of TMCP steel[J]. Transactions of the China Welding Institution, 2004, 30(3): 19 - 23.

[6] 张显辉, 焦 伟, 谭长瑛. 20MnNiMo 钢焊接热影响区的组织和韧性及其氢致裂纹特征[J]. 焊接学报, 2000, 21(3): 9 - 12.
Zhang Xianhui, Jiao Wei, Tan Changying. HAZ structure, toughness and characteristics to hydrogen-induced cracking (HIC) of steel 20MnNiMo[J]. Transactions of the China Welding Institution, 2000, 21(3): 9 - 13.

[7] 毕志超, 张继明, 刘晓东, 等. 核电用高强韧厚规格调质钢板的力学性能和显微结构[J]. 钢铁研究学报, 2011, 10: 10 - 23.
Bi Zhicao, Zhang Jiming, Liu Xiaodong, *et al*. Microstructure and mechanical properties of Q and T heavy plate for nuclear power station purpose[J]. Journal of Iron and Steel Research, 2011, 10: 10 - 23.

[8] 美国机械工程师学会. ASME BPVC-Ⅲ NE-2004 核设施部件建造规则, 第 1 分册, NE 分卷, MC 级部件[S]. 上海: 上海科技文献出版社, 2007.

作者简介: 丁连征,男,1972 年出生,博士. 主要从事焊接技术研究工作. 发表论文 6 篇. Email: dinglz2006@126.com

通讯作者: 孟庆森,男,教授,博士研究生导师. Email: mengqingsen@263.net

are difficult to be conducted. A unified pulsed MIG welding parameters adjusting technology based on least squares method has been proposed in this paper. The optimized fitting curve is achieved and the full advantage of the ideal data that generated in the experiments is utilized by applying a fitting relationship, which obtained through technology experiment, between the large-step welding current and other welding parameters. Besides, easier software program with simple algorithm is realized as well as a wide range of continuous adjustment of the welding parameters. Experiments are conducted after the fitting of single-pulse, double-pulse welding parameters. The experiments results indicate that the welding process is stable to obtain clear fish-scale welding seam with uniformed appearance and fewer spatters. Thus, good stability, reliability and feasibility of the proposed method are well approved.

Key words: least squares method; curve fitting; unified adjustment; digital welder

Crystal orientation in nugget zone of friction stir welded 5083 aluminum alloy plates YUAN Gecheng, LIANG Chunlang, LIU Hong, YUAN Qian (School of Materials and Energy, Guangdong University of Technology, Guangzhou 510006, China). pp 79 – 82

Abstract: The cold rolled 5083 aluminum alloy plates were welded by friction stir welding (FSW). The characteristics of grains orientation evolution in FSW nugget zone(NZ) was researched by electron backscatter diffraction(EBSD) and orientation imaging microscopy(OIM) with analyzing grain characterization, misorientation distribution, textures distribution and orientation distribution function(ODF). The results show that the dynamic recrystallization occurred in NZ due to the effect of heat and deformation which caused a severe plastic flow. Crystal in nugget zone appears to be equiaxed grain with average size 15.8 μm, and fraction of high angle grain boundaries (HAGB) appreciably increased. In the base metal, there were strong Brass texture {011} <211> and S texture {123} <634> that total fractions were above 30.6% and 13.6%, respectively. Conversely, after FSW, B and S textures in the NZ were obviously weakened as total fraction of only 4% and 1.8%, respectively. Furthermore, although the fraction of R texture {124} <211> caused by in-situ recrystallization is up to 7.7%, other common textures in face centered cubic (FCC) metal were weak in the NZ, and every fractions was also below 8%, which means that strong orientation turned into weak orientation in nugget zone.

Key words: 5083 aluminum alloy; friction stir welding; nugget zone; crystal orientation

Test verifies and simulation on welding temperature field of 785 high strength steel for hydraulic support CHI Luxin, SUN Zhaofan, WU Guangfeng (College of Materials Science and Engineering, Chongqing University of Technology, Chongqing, 400050, China). pp 83 – 86

Abstract: The as-received material was subjected to obtain thermal circling curves of typical position by ANSYS software numerical simulation in the different welding technological parameters on 20 mm thick plate to optimize welding process parameters and predict microstructures and properties for improving welding quality, compared with the simulation results and the experimental results in the same welding process conditions. It was found that the values of the thermal circling curves were close to the values measured; the simulation width of welding heat affected zone was basically the same as the measured values; the lath bainite was gradually reduced, the granular bainite increased and the grain size also became coarse from base metal to fusion zone.

Key words: 785 steel; numerical simulation; temperature field; microstructure

Humping and undercutting suppression mechanism for high speed TIG-MIG hybrid welding LOU Xiaofei[1], CHEN Maoai[1], WU Chuansong[1], YE Keli[2] (1. MOE Key Laboratory for Liquid-solid Structure Evolution and Materials processing, Institute for Materials Joining, Shandong University, Jinan 250061, China; 2. Guangxi Technological College of Machinery and Electricity, Nanning 530007, China). pp 87 – 90

Abstract: A TIG-MIG hybrid welding system was set up. A series of experiments on high speed TIG-MIG hybrid welding of low-carbon steel were launched. The effect of TIG-MIG hybrid arc characteristic, droplet transfer mode and the weld pool behavior on weld bead appearance was researched and the welding parameters were optimized. Excellent arc stability and weld appearance were obtained by setting the same value for MIG and TIG currents in the range of 240-300 A. The penetration increased and weld width decreased compared with the traditional MIG welding. Humping or undercutting were suppressed at a high welding speed up to 2.5 m/min The suppression of humping and undercutting defects in TIG-MIG hybrid welding may be attributed to the decrease in hybrid arc pressure due to the interaction between TIG and MIG arc, the disappearance of gouging region and decreases in the weld width.

Key words: TIG-MIG hybrid welding; high speed welding; humping; undercutting.

Weldablity research on the SA738Gr. B steel DING Lianzheng[1], WANG Kai[2], MENG Qingsen[1] (1. Material Science and Engineering Institute., Taiyuan University of Technology, Taiyuan 030024, China; 2. Harbin Welding Institute, China Academy of Machinery Science & Technology, Harbin 150028, China). pp 91 – 94

Abstract: The microstructure transfers were monitored by the expansion tests at the different cooling rates. By using the Gleeble-2000 thermal simulation machine, the impact toughness and the microstructures for the HAZ were also simulated. Furthermore, the weldments were performed to testify the consistency of the simulation specimen and the weldments. The results manifest that with the cooling velocity decreased, the Bainite transfer, the proeutectoid ferrite transfer, and proeutectoid ferrite pearite transfer take place in sequence. Accordingly the mechanical properties decreased. Under the condition of the multipass welds, the HAZ microstructures of the weldments consist of the mixed microstructure, but the base microstructures are same to that of the thermal simulations at the same cooing rate. The research results have a good direction and references to the welding

fabrication.

Key words: SA738Gr. B steel; thermal simulation; heat affected zone; mechanical property

Stress concentration factor equation of heterogeneity joint based on slope angle and material difference XUE Gang[1,2], WANG Tao[2], FANG Hongyuan[1] (1. State Key Laboratory of Advanced Welding and Joining, Harbin Institute of Technology, Harbin 150001, China; 2. Luoyang Ship Material Research Institute, Luoyang 471023, China). pp 95 – 98

Abstract: In order to improve the fatigue load carrying capacity and efficiently predict the fatigue failure position of heterogeneous joint, the influences of groove angle and difference between welded materials on joint stress concentration factor are studied based on finite element method. The weld root stress concentration factor and weld toe stress concentration factor relation equations of flat heterogeneous butt joint are also developed. The result shows that weld root stress concentration factor increases with the increase of groove angle and difference between welded materials, weld toe stress concentration factor decreases with the increase of groove angle and difference between welded materials. The results calculated by stress concentration factor relation equations are in good agreement with the finite element method results, and the relative error is less than 3%.

Key words: weld root stress concentration factor; weld toe stress concentration factor; groove angle; difference between welded materials

Analysis and evaluation of arc stability of self-shielded flux-cored wire in all-position welding ZHANG Tianli[1], LI Zhuoxin[2], JING Hongyang[1], LI Guodong[2], LI Hong[2], SONG Shaopeng[2] (1. School of Materials Science and Engineering, Tianjin University, Tianjin 300072, China; 2. College of Materials Science and Engineering, Beijing University of Technology, Beijing 100124, China). pp 99 – 102

Abstract: The droplet transfer and arc stability of three kinds of self-shielded flux-cored wires in all-position welding applied in X70 pipeline steel were tested by using high-speed video camera and Hanover Analysator. The results showed that as for all-position welding arc stability, No. 1 wire was the best, No. 3 wire the medium, and No. 2 wire the worst; coefficient of current variability could reflect welding stability more accurately than standard deviation; average short-circuiting time could not be taken as the only way to judge welding arc stability, which should be judged by combining with class frequency distributions diagram of short-circuiting time. During short circuiting transfer, probability density distributions diagram of arc voltage was in double-hump shape, and probability density distributions of double-hump shape curve and convergence of the whole curve could be regarded as important references for evaluating welding arc stability.

Key words: self-shielded flux cored wire; all-position welding; droplet transfer; welding arc stability

Microstructure and properties of simulated heat affected zones of weathering heavy steel plate for bridge CHENG Binggui, LIU Dongsheng (Institute of Research of Iron and Steel (IRIS), Shasteel, Zhangjiagang 215625, China). pp 103 – 107, 112

Abstract: Advanced heavy steel plates (60 mm thick) for bridge with room temperature yield-strength greater than 500 MPa and assured low temperature impact toughness (Charpy V notch impact energy (CVN) of 200 J at -40 ℃) have been produced via thermomechanical control process (TMCP). The dependence of microstructure and the impact toughness at -40 ℃ of the coarse-grained heat-affected zone (CGHAZ) generated by single-pass simulated welding upon the heat input energy (E) and peak temperature T_P^2 of simulated second-pass welding processes were revealed. Thermal cycles of the CGHAZ and the sub-regions (intercritically reheated coarse-grained zone (IRCGHAZ), supercritically reheated coarse-grained zone (SRCGHAZ)) of the subject steel plate were simulated employing a Gleeble 3 800 thermomechanical simulator. The microstructure of the CGHAZ consists of lathlike bainite (LB) under E less than 50 kJ/cm. The microstructure changes gradually into granular bainite (GB) associated with coarsened martensite/austenite (M/A) constituents in the cases of E greater than 100 kJ/cm. Ductile impact fracture behavior is observed under the CGHAZ conditions with E less than 100 kJ/cm, while brittle fracture is rendered with E greater than 100 kJ/cm. The IRCGHAZ is the so called local brittle zone (LBZ) under all the tested conditions. This is attributed to the formation of coarse M/A constituents. The SRCGHAZs with moderate and small E which is no greater than 50 kJ/cm show ductile fracture. These are LBZs with increased E which is once again attributed to the formation of GB. The increase of T_P^2 leads to improved impact toughness in the SRCGHAZ. This is attributed to increased hardenability of austenite resulting in transformed-microstructure consisting of fine LB and GB.

Key words: weathering plate steel for bridge; simulated heat affected zones; impact toughness

Effect of welding polar on dry hyperbaric GMAW process LI Kai, GAO Hongming, LI Haichao, DING Yang (State Key Laboratory of Advanced Welding and Joining, Harbin Institute of Technology, Harbin 150001, China). pp 108 – 112

Abstract: Dry hyperbaric gas metal arc welding (GMAW) experiments with direct current electrode positive (DCEP) and direct current electrode negative (DCEN) were carried out. The process characteristics with different welding polar were studied at ambient pressure 0.1 – 2.0 MPa. By using DCEP, welding spatters appears when the pressure reached 0.2 MPa. Spatter generation level increases and spatter size decreases with increasing pressure. When ambient pressure is more than 0.4 MPa, welding process of DCEN is stable with nearly no spatter generation. The characteristics of two spatter types in DCEP were analyzed by high speed camera. The droplet deviated spatter is generated in the process of droplet repelled transfer. Another type of droplet rebounded spatter, is generated by the electromagnetic force. The reason of few spatters generating with DCEN was discwssed.

Key words: dry hyperbaric welding; gas metal arc welding; weld appearance; spatter